

Perceptually informed synthesis of bandlimited classical waveforms using integrated polynomial interpolation

Vesa Välimäki^{a)} and Jussi Pekonen

Aalto University, Department of Signal Processing and Acoustics, Espoo, Finland

Juhan Nam

Stanford University, Center for Computer Research in Music and Acoustics (CCRMA), Stanford, California 94305

(Received 18 June 2010; revised 17 December 2010; accepted 7 March 2011)

Digital subtractive synthesis is a popular music synthesis method, which requires oscillators that are aliasing-free in a perceptual sense. It is a research challenge to find computationally efficient waveform generation algorithms that produce similar-sounding signals to analog music synthesizers but which are free from audible aliasing. A technique for approximately bandlimited waveform generation is considered that is based on a polynomial correction function, which is defined as the difference of a non-bandlimited step function and a polynomial approximation of the ideal bandlimited step function. It is shown that the ideal bandlimited step function is equivalent to the sine integral, and that integrated polynomial interpolation methods can successfully approximate it. Integrated Lagrange interpolation and B-spline basis functions are considered for polynomial approximation. The polynomial correction function can be added onto samples around each discontinuity in a non-bandlimited waveform to suppress aliasing. Comparison against previously known methods shows that the proposed technique yields the best tradeoff between computational cost and sound quality. The superior method amongst those considered in this study is the integrated third-order B-spline correction function, which offers perceptually aliasing-free sawtooth emulation up to the fundamental frequency of 7.8 kHz at the sample rate of 44.1 kHz.

© 2012 Acoustical Society of America. [DOI: 10.1121/1.3651227]

PACS number(s): 43.75.Wx, 43.75.Zz [MAH]

Pages: 974–986

I. INTRODUCTION

Digital subtractive synthesis refers to the emulation of analog music synthesis using a computer and it is one of the popular synthesis methods nowadays. The sound-generation principle in subtractive synthesis is first to synthesize a signal with rich spectral content and then to filter that signal with a time-varying filter. There is a tradition^{1,2} to use geometric periodic signals, such as the sawtooth, the rectangular, or the triangle waveform, as the source. Annoyingly, digital synthesis of these classical waveforms via trivial sampling suffers from aliasing distortion that can be heard as a disturbing hiss, hum, or beating.^{3–6} This is due to the discontinuities in the waveforms, or their derivatives, which require a nearly infinite bandwidth in the frequency domain. The challenge, and the topic of this paper, is to devise an efficient digital signal generation algorithm, which is free from audible aliasing and produces similar-sounding signals to analog music synthesizers.

In principle, the aliasing in the audio band can be reduced by increasing the sample rate.^{6,7} However, since the spectra of periodic waveforms decay gently, for example, at only about 6 dB per octave in the case of the sawtooth signal, a very high oversampling ratio is required for proper aliasing suppression. More advanced approaches that have been suggested are briefly reviewed next.

The earliest approaches in the 1970s reduced a sum of harmonically related sinusoids into a fraction of two trigonometric functions using the properties of the sine and cosine functions.^{8,9} These methods correspond to a condensed implementation of additive synthesis.¹⁰ Another perspective on the additive synthesis of the classical waveforms is specifying their spectral content in the frequency domain and then applying the inverse (fast) Fourier transform to the synthesized spectrum.¹¹ A common approach to producing a fixed number of harmonically related sinusoids is to utilize wavetable synthesis,^{5,7} where a precomputed table containing one cycle of an oscillation is played back. By reading the look-up table at a different rate, the fundamental frequency of the waveform is changed from its nominal value.¹²

Alternatively, the waveforms can be synthesized from a sinusoid by means of distortion synthesis^{13–15} in which the higher harmonics are generated by applying a nonlinear waveshaper^{16,17} or phase distortion^{18,19} to the sinusoid having the desired fundamental frequency. The phase distortion approach using a time-varying first-order allpass filter^{14,19,20} has been extended to a chain of time-varying allpass filters.²¹ Other nonlinear approaches to the approximation of these classical waveforms include the use of a nonlinear waveshaper in the feedback path of a feedback amplitude modulation synthesizer²² and bitwise logical modulation of two sinusoidal oscillators.²³ However, although one can obtain nearly bandlimited waveforms with these nonlinear approaches, it should be noted that they are generally not bandlimited.

^{a)}Author to whom correspondence should be addressed. Electronic mail: vesa.valimaki@tkk.fi

The bandlimited waveforms can be approximated with the help of a signal that has a spectrum containing the harmonics of the target waveform but with a steeper spectral tilt. A digital filter can then be used to modify the overall spectral shape to obtain close approximations of the classical waveforms. One such approach produces the sawtooth wave by full-wave rectifying a sine wave of half of the target fundamental frequency and by applying a tracking highpass filter and a fixed lowpass filter to the rectified sinusoid.²⁴ A related recent approach generates the sawtooth waveform by differentiating a piecewise parabolic waveform, i.e., a squared sawtooth wave signal.^{25–27} The other classical waveforms are obtained with modifications to the basic algorithm.²⁷ It is possible to obtain the rectangular pulse and the skewed triangle waveshapes by FIR comb filtering^{6,28} the sawtooth wave and piecewise parabolic signals, respectively. This differentiated second-order polynomial waveform approach has recently been extended to higher-order differentiations of higher-order polynomials.²⁹ The aliasing has been shown to be reduced also by highpass and comb filtering the alias-corrupted signals.³⁰

Stilson and Smith suggested in 1996 an approach that is based on bandlimiting the derivative of the waveform.³¹ By bandlimiting the waveform derivative, i.e., by replacing each lone impulse, the derivative of a waveform discontinuity, with the impulse response of a lowpass filter, and by applying integration to the resulting bandlimited impulse train (BLIT), an approximately bandlimited waveform is obtained.^{31,32} Here the integration and differentiation only vary the spectral tilt of the waveform by increasing and decreasing it, respectively, by about 6 dB per octave, as can be proven by analyzing the Laplace transforms of the derivative and the integral of a signal. Approximations of the bandlimited impulses used in the BLIT approach have been proposed, including modified frequency modulation,³³ feedback delay loops,^{34,35} the impulse responses of low-order fractional delay filters,^{35,36} parametric window functions,³⁷ and optimized look-up table designs.³⁷

However, the integration in the BLIT approach may cause numerical problems when it is implemented with finite accuracy.^{32,36} In order to avoid this issue, Brandt proposed the use of a second-order leaky integrator that has zero DC gain.³⁸ Furthermore, he suggested that the numerical problems could be overcome by performing the integration beforehand by using an accumulated impulse response of the lowpass filter. When every step-like discontinuity of the waveform is replaced with the accumulated impulse response, that Brandt calls a bandlimited step function (BLEP), an approximately bandlimited waveform is obtained.³⁸

Both the BLIT and the BLEP methods are usually implemented by sampling the impulse response of a continuous-time lowpass filter³⁹ that is further accumulated in the BLEP approach. The latter approach leads to an approximation of the ideal bandlimited unit step function. In this paper, the ideal bandlimited unit step function is derived in closed form.

The BLIT and the BLEP methods require a table in which the sampled impulse response or the sampled accumulated impulse response is stored.^{31–33,38–40} In practice, the impulse response of the lowpass filter must be oversampled in order to achieve improved accuracy in the positioning of

the waveform transition between the sampling points. This raises another issue since large tables cannot be used in memory sensitive platforms. In order to achieve good accuracy, the oversampling factor should be large, for example, 32, which makes the table size even larger. This paper proposes a polynomial approximation of the ideal bandlimited unit step function based on integrated Lagrange or B-spline interpolation. These methods lead to a computationally efficient implementation of the BLEP method that does not require a table or oversampling.

At high fundamental frequencies, when K samples around each discontinuity are corrected using the table-based BLEP method, two or more tables may overlap, since the distance between contiguous discontinuities can be less than K samples. The same problem occurs also with the table-based BLIT method. Taking care of overlapping tables increases the computational cost per output sample. If the overlapping is undesirable and must be avoided, the highest possible fundamental frequency for a synthetic sawtooth signal using the table-based BLEP and BLIT approaches is then f_s/K , where f_s is the sample rate.¹³ The methods proposed in this paper use low-order polynomials, which correspond to shorter correction functions (i.e., a smaller K) than when a table is used.

Section II of this paper shows that the ideal BLEP function is equivalent to the well-known sine integral. The use of the BLEP residual function in the synthesis of the classical waveforms is explained and illustrated. The polynomial approximation of the ideal BLEP function using integrated Lagrange and B-spline interpolation is discussed in Sec. III. The proposed polynomial waveform correction approaches are evaluated in Sec. IV where the audibility of the produced aliasing is investigated using a model of auditory masking and a standard perceptual sound quality measure. In addition, the computational load of the proposed approaches is discussed. A comparison with alternative waveform synthesis methods is presented. Section V concludes the paper.

II. BANDLIMITED STEP FUNCTIONS

The continuous-time classical waveforms can be constructed by integrating the sum of an impulse train and a constant.^{31,32,34,36} This is equivalent to summing a sequence of unit step functions and a linear function.³⁸ These approaches lead to the previously proposed BLIT and BLEP synthesis methods, respectively, when bandlimited versions of the basis functions are used. Using the summing of unit step functions, the rectangular pulse wave with a fundamental frequency $f_0 = 1/T_0$ and a duty cycle, or the pulse width, P can be expressed as

$$r(t; P) = 2 \sum_{k=-\infty}^{\infty} [u(t - kT_0) - u(t - (k + P)T_0)] - 1, \quad (1)$$

where $u(x)$ is the Heaviside unit step function given by

$$u(x) = \int_{-\infty}^x \delta(\tau) d\tau = \int_{0-}^x \delta(\tau) d\tau = \begin{cases} 0, & \text{when } x < 0, \\ 0.5, & \text{when } x = 0, \\ 1, & \text{when } x > 0 \end{cases} \quad (2)$$

and $\delta(t)$ is the Dirac delta (impulse) function. The sawtooth wave can be expressed as

$$s(t) = 1 + \frac{2t}{T_0} - 2 \sum_{k=-\infty}^{\infty} u(t - kT_0) \quad (3)$$

and the triangle wave as

$$s(t) = \frac{4}{T_0} \int_{-\infty}^t r(\tau; 0.5) d\tau = \frac{8}{T_0} \sum_{k=-\infty}^{\infty} ((t - kT_0)u(t - kT_0) - (t - (k + 0.5)T_0)u(t - (k + 0.5)T_0)) - 1. \quad (4)$$

In the ideal BLIT method, the synthesis algorithm first smooths the impulse train with an ideal lowpass filter, i.e., a filter that passes the frequencies below a cut-off frequency as is and blocks the frequencies above it.^{31,32} Every unit impulse is replaced with the impulse response of the ideal lowpass filter given by

$$h_{\text{id}}(t) = \alpha f_s \text{sinc}(\alpha f_s t), \quad (5)$$

where f_s is the sample rate, $0 \leq \alpha \leq 1$ is a scaling factor for the filter cut-off frequency, and $\text{sinc}(x) = \sin(\pi x)/(\pi x)$.

In the BLEP method, each step-like discontinuity in the signal is replaced with a bandlimited unit step function, which is the integral of the bandlimited impulse, i.e., the impulse response of the ideal lowpass filter. Previously accumulating a windowed impulse response has approximated the integration since the sinc function itself is infinitely long. However, the ideal bandlimited unit step function can be expressed in closed form as

$$\begin{aligned} h_{\text{id}}(t) &= \int_{-\infty}^t h_{\text{id}}(\tau) d\tau = \alpha f_s \int_{-\infty}^t \frac{\sin(\pi \alpha f_s \tau)}{\pi \alpha f_s \tau} d\tau \\ &= \frac{1}{\pi} \int_{-\infty}^{\pi \alpha f_s t} \frac{\sin(\tau)}{\tau} d\tau = \frac{1}{\pi} \int_{-\pi \alpha f_s t}^{\infty} \frac{\sin(\tau)}{\tau} d\tau \end{aligned} \quad (6)$$

from which by substituting

$$\text{si}(x) = - \int_x^{\infty} \frac{\sin(t)}{t} dt = \text{Si}(x) - \frac{\pi}{2}, \quad (7)$$

$$\text{Si}(x) = \int_0^x \frac{\sin(t)}{t} dt = \sum_{n=0}^{\infty} \frac{(-1)^n x^{2n+1}}{(2n+1)(2n+1)!}, \quad (8)$$

$$\text{Si}(-x) = -\text{Si}(x), \quad (9)$$

where $\text{Si}(x)$ is the well-known sine integral,⁴¹ yields

$$\begin{aligned} h_{\text{id}}(t) &= -\frac{1}{\pi} \text{si}(-\pi \alpha f_s t) = -\frac{1}{\pi} \left(\text{Si}(-\pi \alpha f_s t) - \frac{\pi}{2} \right) \\ &= \frac{1}{2} + \frac{1}{\pi} \text{Si}(\pi \alpha f_s t). \end{aligned} \quad (10)$$

Now, since the sawtooth and the rectangular pulse wave can be synthesized by summing time-shifted unit step functions, the respective bandlimited waveforms can be constructed by replacing every unit step function with the bandlimited unit step $h_{\text{id}}(t)$ function derived above.

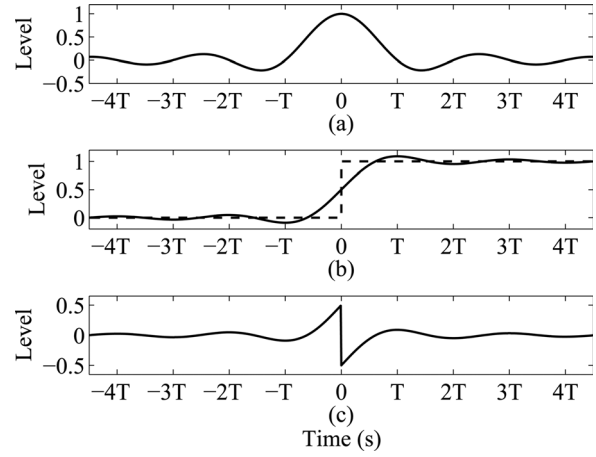


FIG. 1. When the continuous-time sinc pulse in (a) is integrated, the ideal bandlimited step function, the sine integral, shown in (b) (solid line) is obtained. The unit step function is also shown in (b) (dashed line). The BLEP residual, the difference between the bandlimited step function and the unit step function, is plotted in (c). T is the sampling interval used, i.e., $T = 1/f_s$.

The forming of the correction function used in the BLEP approach for the sawtooth and the rectangular pulse wave is illustrated in Fig. 1, where the impulse response of the ideal lowpass filter, the ideal bandlimited unit step function, and the BLEP residual are shown for the cut-off frequency-scaling factor $\alpha = 1$. The correction function, called the BLEP residual, is the difference between the bandlimited unit step function $h_{\text{id}}(t)$ and the unit step function $u(t)$. Samples taken from the BLEP residual [see Fig. 1(c)] can be summed onto each discontinuity of a trivially sampled signal, resulting in a computationally efficient implementation of the synthesis algorithm.

In case of the triangle wave, however, the replacement of each unit step function with a bandlimited step function is inadequate. Here, the ramp functions of Eq. (4), i.e., terms of form $\tau u(\tau)$ need to be replaced with the integral of the bandlimited step function, given by

$$\int h_{\text{id}}(t) dt = t h_{\text{id}}(t) + \frac{\cos(\pi \alpha f_s t)}{\pi^2 \alpha f_s}. \quad (11)$$

Figure 2 illustrates how a trivially sampled rectangular pulse signal can be post-processed using the BLEP method. Figure 2(b) shows the correction functions associated with each discontinuity in the trivial pulse signal of Fig. 2(a). In this example, the BLEP residual modifies only six samples, three before and three after the transition. The truncated correction functions in Fig. 2(b) have been shifted by the fractional delay of each discontinuity, i.e., the delay between the discontinuity and the sample following it, and have then been sampled at the six regular sampling grid points from the ideal BLEP residual. Note that this method requires detection of the accurate location of each discontinuity in the original signal between the sampling instants.

Additionally, the magnitude and direction (up or down) of each discontinuity must be estimated because the polarity and amplitude of the correction function depend on them. In this example all discontinuities have the same magnitude

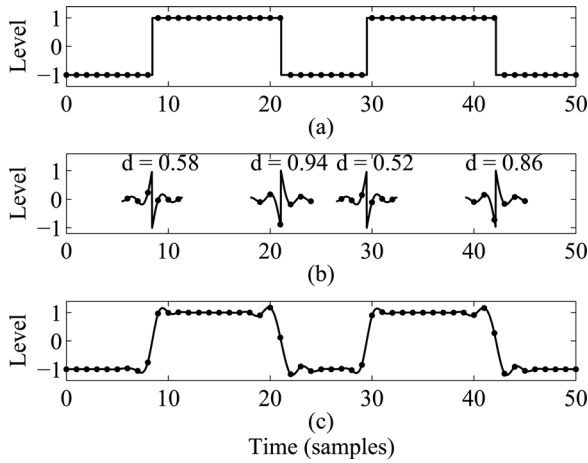


FIG. 2. (a) Continuous-time (solid line) and trivially sampled (dots) rectangular signal, (b) truncated BLEP residual functions of length $6T$ (solid line) centered at each discontinuity and inverted for downward steps, and (c) an approximately bandlimited signal that is obtained by adding sampled signals (a) and (b). The fractional delay associated with each discontinuity is given in (b).

(2.0), but their polarity varies. For this reason, every second correction function in Fig. 2(b) has been inverted. Figure 2(c) shows the sum of the original signal and the correction function samples. This process results in an approximately bandlimited version of the original signal.

The corresponding fractional delay of each discontinuity can be computed using the principle of similar right triangles, as depicted in Fig. 3. Since a unipolar modulo counter can be used to compute the instantaneous phase of the waveform, the fractional delay can be directly computed from the value of the modulo counter after the discontinuity. For simplicity, assume that the values of the modulo counter are limited to be between 0 and 1, since any modulo counter can be normalized to satisfy this assumption. Now, for the waveform phase reset, see Fig. 3(a), the relation

$$\frac{p(n)}{Td} = \frac{f_0T}{T}, \quad (12)$$

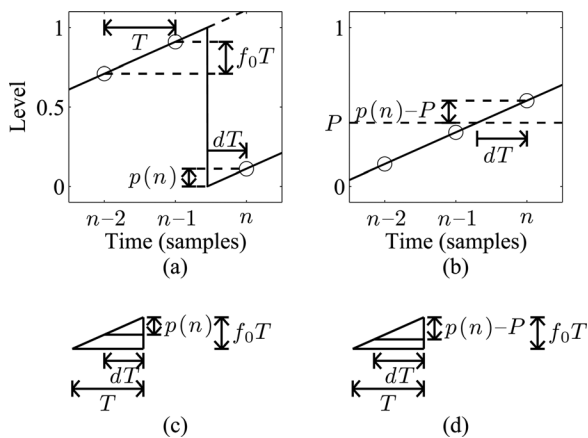


FIG. 3. Principle for computing the fractional delay d for the localization of the BLEP residual (a) at the start of a new fundamental period and (b) at the downward shift of the rectangular pulse wave with duty cycle P . The step size f_0T and the sampling interval T form the sides of a right triangle which is similar to the right triangles from which fractional delay d can be solved for (c) a sawtooth wave or (d) a rectangular pulse wave.

where $p(n)$ is the modulo counter value after the discontinuity, d corresponds to the fractional delay, T is the sampling interval, and f_0T is the step size of the counter, is obtained from Fig. 3(c). Thus, the fractional delay can be solved as

$$d = \frac{p(n)}{f_0T}. \quad (13)$$

In the case of a rectangular pulse wave, the fractional delay associated with the downward discontinuity is computed from the value of the modulo counter after it exceeds P , the duty cycle [see Fig. 3(b)]. However, in this case P needs to be subtracted from the modulo counter value, as shown in Fig. 3(d), in order to obtain the correct fractional delay value. When generating a triangle wave, the fractional delays of the turning points are obtained similarly with $P = 0.5$.

III. CORRECTION BASED ON POLYNOMIAL INTERPOLATION

Next, a polynomial approximation of the ideal BLEP method, originally proposed by Välimäki and Huovilainen,³⁹ is discussed. Previously, the basis function of linear interpolation, i.e., a continuous-time triangle pulse, was integrated with respect to time in order to obtain a closed-form, second-order polynomial approximation of the bandlimited step function.³⁹ In addition, the integrals of a third-order spline and a truncated third-order Lagrange interpolator that modifies only the two samples that precede and follow a discontinuity have been previously used as the approximately bandlimited step function.¹³ This section extends this idea to general N th-order interpolation polynomials, yielding an $(N + 1)$ th-order polynomial bandlimited step function called PolyBLEP. The order of the PolyBLEP function is denoted by N_I .

A. Integrated Lagrange interpolation

Lagrange interpolation is commonly used to interpolate bandlimited signals, such as in sampling-rate conversions or in fractional-delay filtering.^{42–46} The N th-order Lagrange interpolation coefficients can be expressed in closed form as

$$\begin{aligned} h_L(n) &= \prod_{\substack{k=0 \\ k \neq n}}^N \frac{D-k}{n-k} = \prod_{\substack{k=0 \\ k \neq n}}^N \frac{1}{n-k} \times \prod_{\substack{k=0 \\ k \neq n}}^N (D-k) \\ &= C(n) \prod_{\substack{k=0 \\ k \neq n}}^N (D-k) \end{aligned} \quad (14)$$

for $n = 0, 1, 2, \dots, N$, where D is a real number that corresponds to the delay from the beginning ($n = 0$) of the impulse response and $C(n)$ are constant scaling coefficients.^{45,47} An FIR filter with the above coefficients $h_L(n)$ shifts the input signal by approximately D sampling intervals.

It has been shown previously that the Lagrange interpolation is a maximally flat approximation of sinc interpolation around the zero frequency.⁴⁷ Knowing this, integrated Lagrange interpolation, which is an approximation of the sine

TABLE I. First-order ($N = 1$) Lagrange polynomials, their integrated forms, and the corresponding BLEP residual polynomials, which correspond to the shifted integrated Lagrange polynomials from which a unit step function has been subtracted. Span refers to the time interval on which each polynomial is applied. Time 0 refers to the mid-point of the correction function and T is the sampling interval.

Span	Lagrange polynomial ($0 \leq D < 1$)	Integrated Lagrange polynomial ($0 \leq D < 1$)	BLEP residual ($0 \leq d < 1$)
$-T \dots 0$	D	$D^2/2$	$d^2/2$
$0 \dots T$	$-D + 1$	$-D^2/2 + D + 1/2$	$-d^2/2 + d - 1/2$

integral (i.e., the integrated sinc function), is defined. The integral of the Lagrange interpolation formula with respect to D can be written as

$$h_{\text{IL}}(n) = \int h_{\text{L}}(n) dD + E_{\text{L}}(n), \quad (15)$$

where $h_{\text{L}}(n)$ is the Lagrange interpolation coefficient given by Eq. (14) and $E_{\text{L}}(n)$ is a constant with which the integrated Lagrange interpolation polynomials are set to be continuous. These constants are selected so that the polynomial begins from the zero level and the polynomials for the successive coefficients are continuous at their boundaries. For a chosen polynomial of order N , the coefficient $h_{\text{IL}}(n)$ can be computed as described above. The computed polynomial is evaluated for delay D and an approximation of the ideal BLEP function is obtained. To obtain an approximation of the ideal BLEP residual, a unit step function $u(n)$ must be subtracted from Eq. (15).

Tables I, II, and III show the formulae for three low-order Lagrange polynomials. The interpolation polynomials were obtained by evaluating Eq. (14) for orders 1, 2, and 3, respectively. The integrated polynomials were obtained by integrating the interpolation polynomials with respect to D and by setting the polynomials to be continuous, as described above. Integration increases the orders of these polynomials

TABLE II. Second-order ($N = 2$) Lagrange polynomials, their integrated forms, and the corresponding BLEP residuals.

Span	Lagrange polynomial ($0.5 \leq D < 1.5$)
$-1.5T \dots -0.5T$	$D^2/2 - D/2$
$-0.5T \dots 0.5T$	$-D^2 + 2D$
$0.5T \dots 1.5T$	$D^2/2 - 3D/2 + 1$
Span	Integrated Lagrange polynomial ($0.5 \leq D < 1.5$)
$-1.5T \dots -0.5T$	$D^3/6 - D^2/4 + 1/24$
$-0.5T \dots 0.5T$	$-D^3/3 + D^2 - 1/6$
$0.5T \dots 1.5T$	$D^3/6 - 3D^2/4 + D + 5/8$
Span	BLEP residual ($0 \leq d < 1$)
$-1.5T \dots -T$	$d^3/6 - d^2/4 + 1/24$, when $0.5 \leq d < 1$
$-T \dots -0.5T$	$d^3/6 + d^2/4 - 1/24$, when $0 \leq d < 0.5$
$-0.5T \dots 0$	$-d^3/3 + d^2 - 1/6$, when $0.5 \leq d < 1$
$0 \dots 0.5T$	$-d^3/3 + d - 1/2$, when $0 \leq d < 0.5$
$0.5T \dots T$	$d^3/6 - 3d^2/4 + d - 3/8$, when $0.5 \leq d < 1$
$T \dots 1.5T$	$d^3/6 - d^2/4 + 1/24$, when $0 \leq d < 0.5$

TABLE III. Third-order ($N = 3$) Lagrange polynomials, their integrated forms, and the corresponding BLEP residual polynomials.

Span	Lagrange polynomial ($1 \leq D < 2$)
$-2T \dots -T$	$D^3/6 - D^2/2 + D/3$
$-T \dots 0$	$-D^3/2 + 2D^2 - 3D/2$
$0 \dots T$	$D^3/2 - 5D^2/2 + 3D$
$T \dots 2T$	$-D^3/6 + D^2 - 11D/6 + 1$
Span	Integrated Lagrange polynomial ($1 \leq D < 2$)
$-2T \dots -T$	$D^4/24 - D^3/6 + D^2/6 - 1/24$
$-T \dots 0$	$-D^4/8 + 2D^3/3 - 3D^2/4 + 1/6$
$0 \dots T$	$D^4/8 + 5D^3/6 + 3D^2/2 - 7/24$
$T \dots 2T$	$-D^4/24 + D^3/3 - 11D^2/12 + D + 2/3$
Span	BLEP residual ($0 \leq d < 1$)
$-2T \dots -T$	$d^4/24 - d^2/12$
$-T \dots 0$	$-d^4/8 + d^3/6 + d^2/2 - 1/24$
$0 \dots T$	$d^4/8 - d^3/3 - d^2/4 + d - 1/2$
$T \dots 2T$	$-d^4/24 + d^3/6 - d^2/6 + 1/24$

by one. Lastly, the polynomial correction functions associated with integrated first-, second- and third-order Lagrange interpolation polynomials are also presented in Tables I, II, and III, respectively. A unit step function centered at the discontinuity was subtracted from the integrated interpolation polynomial, and a variable change was implemented so that each polynomial segment can be computed using the fractional delay d , i.e., the fractional part of the delay D .

For odd-order interpolation polynomials, the variable change is obtained with $d = D - (N - 1)/2$. When the order of the interpolation polynomial is even, the substitution is more complicated. Now, since the polynomial is applied asymmetrically with respect to the discontinuity depending on its position, two cases are obtained: the discontinuity is either located closer to the sampling instant before or after it. In the first case, the correction function is applied to $N/2 + 1$ samples before and $N/2$ samples after the discontinuity, whereas in the latter case the numbers of samples to be modified before and after the discontinuity are interchanged. When the discontinuity is closer to the sampling instant before it, the fractional delay should lie in the range $0.5 \leq d < 1$ (cf. Fig. 3). This can be obtained by substituting $d = D - N/2 - 1$. In the other case, the fractional delay is in the range $0 \leq d < 0.5$, which yields a substitution $d = D - N/2$. This also means that the correction functions are different for these two cases, as can be seen in Table II.

The continuous-time impulse response, the integrated impulse response, and the PolyBLEP residual of first-, second-, and third-order Lagrange interpolators are depicted in Fig. 4. As can be seen from Figs. 4(a), 4(d), and 4(g), the impulse responses of the interpolation polynomials give a closer approximation of the sinc function as the interpolation order increases. Similarly, as the interpolation order increases, the PolyBLEP residual functions, shown in Figs. 4(c), 4(f), and 4(i), resemble more the ideal BLEP residual function [cf. Fig. 1(c)].

Figure 5 shows the waveforms and spectra of bandlimited sawtooth signal approximations using the proposed

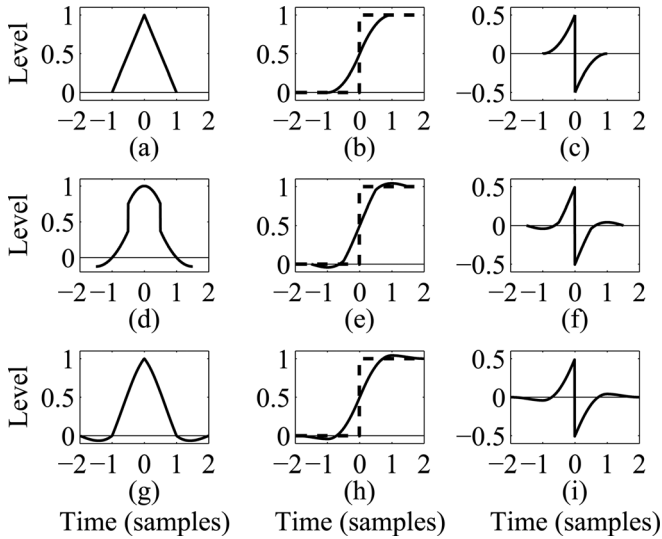


FIG. 4. Continuous-time impulse responses of the (a) first-order, (d) second-order, and (g) third-order Lagrange interpolation, their corresponding integrated impulse responses (solid line) together with the unit step function (dashed line) in (b), (e), and (h), and their differences, i.e., polynomial approximations of the BLEP residual function, in (c), (f), and (i), respectively.

method. The waveforms have been obtained by modifying the trivial sawtooth waveform, i.e., the output signal of a bipolar modulo counter. The modification involves the addition of samples from the PolyBLEP residual function. It is seen that differences between waveforms in Figs. 5(a), 5(c), and 5(e) are small. However, the aliasing in the magnitude spectrum becomes more attenuated as the interpolation order is increased, as seen in Figs. 5(b), 5(d), and 5(f).

The crosses in Fig. 5 show the harmonic levels for the ideal sawtooth signal. It is seen that the desired harmonic components at high frequencies are slightly reduced.

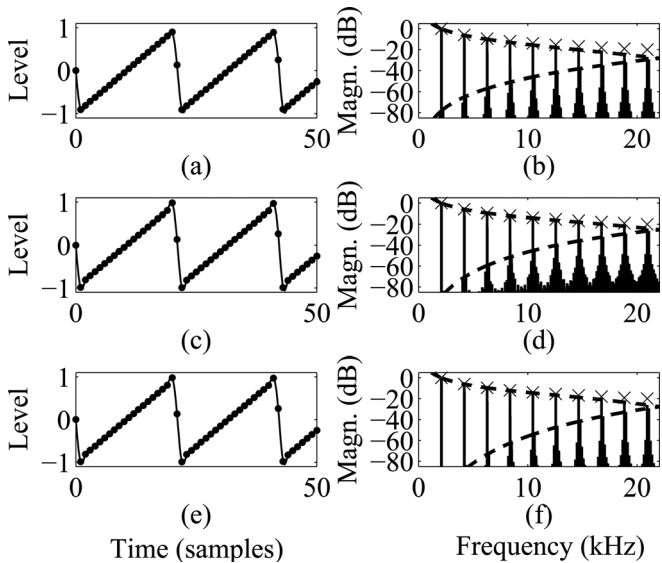


FIG. 5. Sawtooth waveforms produced by the (a) second-order, (c) third-order, and (e) fourth-order Lagrange PolyBLEP approaches and their respective magnitude spectra (b), (d), and (f). The crosses indicate the nominal levels of harmonics of the sawtooth wave. The dashed lines show the spectral envelope of the synthetic harmonics and the first generation of aliased spectral components in each case.

TABLE IV. Coefficients b_0 and b_1 of the second-order post-processing equalizing FIR filter [see Eq. (16)] for the proposed algorithms.

Approach	PolyBLEP order	b_0	b_1
Lagrange	$N_1=2$	-0.1469	1.2674
	$N_1=3$	-0.0435	1.0682
	$N_1=4$	-0.0721	1.1130
B-spline	$N_1=3$	-0.2424	1.4345
	$N_1=4$	-0.3564	1.6292

amplitudes of the higher harmonics are to be restored to the desired level, a post-processing equalizing filter can be used.³⁷ In practice, a low-order filter, which is independent of the fundamental frequency, will suffice to restore the harmonics to be very close to the desired levels. Table IV shows the optimized parameters of a second-order linear-phase FIR filter expressed as

$$H_{\text{eq}}(z) = b_0 + b_1 z^{-1} + b_0 z^{-2}, \quad (16)$$

where b_0 and b_1 are the filter coefficients, for the Lagrange polyBLEP algorithms of orders 2, 3, and 4. This filter corrects the amplitudes of all harmonic components below 15 kHz to be within 1.0 dB of their desired levels.

The spectral envelope of the Lagrange PolyBLEP residual can be expressed in closed form by exploiting the frequency response of the N th-order Lagrange interpolation recently derived by Franck and Brandenburg.⁴⁸ Since the frequency response of an integrated signal is the frequency response of the underlying signal divided by the (angular) frequency (cf. discussion on the BLIT method in Sec. I), the spectral envelope of the Lagrange PolyBLEP is the spectral envelope of the respective interpolation polynomial divided by the frequency. Further, the spectral envelope of the Lagrange PolyBLEP residual is obtained by subtracting the frequency response of the unit step, $1/(j\omega)$, where ω is the angular frequency, from the frequency response of the Lagrange PolyBLEP. The spectral envelopes for the second-, third-, and fourth-order Lagrange PolyBLEP functions are listed in Table V. The baseband and the first generation of aliased components of these responses are plotted in Figs. 5(b), 5(d), and 5(f), where the dashed line illustrates the spectral envelopes of the signal and the first generation of aliasing.

It can be seen in Fig. 5 that increasing the PolyBLEP order from an even order to the next odd order does not improve the alias reduction performance much, especially at low frequencies where the aliasing is more easily perceivable. Furthermore, as the computation of the correction function depends on the range of the fractional delay in all odd-order Lagrange PolyBLEPs, the small improvement in alias

TABLE V. Spectral envelopes of second-, third-, and fourth-order Lagrange PolyBLEP functions.

PolyBLEP order	Spectral envelope
$N_1=2$	$\text{sinc}^2(\omega/2\pi)/\omega$
$N_1=3$	$(1 + \omega^2/8) \text{sinc}^3(\omega/2\pi)/\omega$
$N_1=4$	$(1 + \omega^2/6) \text{sinc}^4(\omega/2\pi)/\omega$

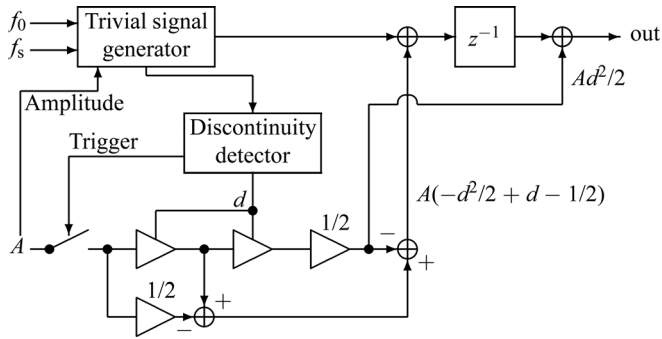


FIG. 6. Signal-processing structure that implements the polynomial correction of a trivial waveform, such as a rectangular signal. The polynomial BLEP method based on the integrated first-order Lagrange interpolation (see Table I) is shown.

reduction is obtained with a larger increase in the computational complexity of the algorithm. More generally, the odd-order Lagrange PolyBLEPs are computationally at least as complex as the next even-order Lagrange PolyBLEP due to the additional control logic that is required to select the polynomials to be evaluated. Therefore, the use of even-order Lagrange PolyBLEPs is highly recommended, i.e., an odd-order interpolation polynomial is used as the starting point of the algorithm.

In Fig. 6, a signal-processing structure that implements the integrated first-order Lagrange interpolator is illustrated. This algorithm has minimal memory allocation, as look-up tables are not needed. The structure is optimized so that the number of required operations is as low as possible by combining common terms of both coefficients. This configuration utilizes multiplications by $1/2$, which can be efficiently implemented on a signal processor. Additionally, one of the polynomials to be evaluated is sparse in the sense that the coefficients of some terms are zero, see also Table I. Thus, the evaluation of these two second-order polynomials requires less computing than the evaluation of two second-order polynomials in general. Similarly, the BLEP residual polynomials in the third- and fourth-order cases are sparse, see Tables II and III.

The discontinuity detector in Fig. 6 looks for major differences between two neighboring samples in the input signal provided by the trivial signal generator. Every time a discontinuity is found, its fractional delay d and height (i.e., level) A are determined, and the detector then initiates (i.e., triggers) the correction function generation by feeding a unit impulse multiplied by A into the structure. The structure then computes the required two polynomial correction function samples and adds them onto the input signal samples, as shown in Fig. 6. The location of the discontinuity is accurately accounted for by the fractional delay value d , and the oversampling needed in table-based BLEP approaches is thus avoided.

B. Integrated B-spline interpolation

B-splines are another family of polynomial functions for interpolating discrete signals and are often used in image processing.⁴⁹ The B-spline polynomials $\beta_N(x)$ of order N are

constructed from $(N + 1)$ -fold convolutions of a rectangular pulse $\beta_0(x)$, i.e.,

$$\beta_0(x) = \begin{cases} 1, & |x| \leq 0.5, \\ 0, & \text{otherwise,} \end{cases} \quad (17)$$

$$\beta_N(x) = \beta_0(x) * \beta_{N-1}(x), \quad \text{for } N = 1, 2, \dots \quad (18)$$

As a result, $\beta_N(x)$ is expressed as a piece-wise polynomial similarly to the Lagrange interpolation polynomials. It should be noted that the first-order B-spline polynomial is identical to the first-order Lagrange interpolation polynomial, which is commonly known as linear interpolation.

An FIR filter that shifts the input signal by approximately D sampling intervals using the B-spline interpolation can be expressed as $h_B(n) = \beta_N(D-n)$. As with the Lagrange interpolation, the integral of the B-spline interpolation formula with respect to D is written as

$$h_{IB}(n) = \int h_B(n) dD + E_B(n), \quad (19)$$

where $E_B(n)$ is a constant with which the successive integrated B-spline interpolation coefficients are set to be continuous at their boundaries. The B-spline PolyBLEP residual function can be obtained by subtracting a unit step function from Eq. (19). Tables VI and VII show the coefficients of B-spline polynomials $h_B(n)$, their integrated forms, and the polynomial correction functions with respect to D and d for orders 2 and 3, respectively. They were evaluated in the same way as the Lagrange interpolation with the difference that the polynomials are given by Eqs. (17), (18), and (19). Again it is seen that some of the resulting polynomials in Tables VI and VII are sparse, and some of their coefficients are trivial, such as $\pm 1/2$.

The second- and third-order B-spline polynomials, their integrated forms, and the respective PolyBLEP residuals are depicted in Fig. 7. Figures 7(a) and 7(d) show that the B-spline interpolation polynomials form bell shapes with

TABLE VI. Second-order ($N=2$) B-spline polynomials, their integrated forms, and the corresponding BLEP residuals.

Span	B-spline polynomial ($0.5 \leq D < 1.5$)
$-1.5T \dots -0.5T$	$D^2/2 - D/2 + 1/8$
$-0.5T \dots 0.5T$	$-D^2 + 2D - 1/4$
$0.5T \dots 1.5T$	$D^2/2 - 3D/2 + 9/8$
Span	Integrated B-spline polynomial ($0.5 \leq D < 1.5$)
$-1.5T \dots -0.5T$	$D^3/6 - D^2/4 + D/8 - 1/48$
$-0.5T \dots 0.5T$	$-D^3/3 + D^2 - D/4 + 1/12$
$0.5T \dots 1.5T$	$D^3/6 - 3D^2/4 + 9D/8 + 7/16$
Span	BLEP residual ($0 \leq d < 1$)
$-1.5T \dots -T$	$d^3/6 - d^2/4 + d/8 - 1/48$, when $0.5 \leq d < 1$
$-T \dots -0.5T$	$d^3/6 + d^2/4 + d/8 + 1/48$, when $0 \leq d < 0.5$
$-0.5T \dots 0$	$-d^3/3 + d^2 - d/4 + 1/12$, when $0.5 \leq d < 1$
$0 \dots 0.5T$	$-d^3/3 + 3d/4 - 1/2$, when $0 \leq d < 0.5$
$0.5T \dots T$	$d^3/6 - 3d^2/4 + 9d/8 - 9/16$, when $0.5 \leq d < 1$
$T \dots 1.5T$	$d^3/6 - d^2/4 + d/8 - 1/48$, when $0 \leq d < 0.5$

TABLE VII. Third-order ($N=3$) B-spline polynomials, their integrated forms, and the corresponding BLEP residual polynomials.

Span	B-spline polynomial ($1 \leq D < 2$)
$-2T \dots -T$	$D^3/6 - D^2/2 + D/2 - 1/6$
$-T \dots 0$	$-D^3/2 + 2D^2 - 2D + 2/3$
$0 \dots T$	$D^3/2 - 5D^2/2 + 7D/2 - 5/6$
$T \dots 2T$	$-D^3/6 + D^2 - 2D + 4/3$
Span	Integrated B-spline polynomial ($1 \leq D < 2$)
$-2T \dots -T$	$D^4/24 - D^3/6 + D^2/4 - D/6 + 1/24$
$-T \dots 0$	$-D^4/8 + 2D^3/3 - D^2 + 2D/3 - 1/6$
$0 \dots T$	$D^4/8 - 5D^3/6 + 7D^2/4 - 5D/6 + 7/24$
$T \dots 2T$	$-D^4/24 + D^3/3 - D^2 + 4D/3 + 1/3$
Span	BLEP residual ($0 \leq d < 1$)
$-2T \dots -T$	$d^4/24$
$-T \dots 0$	$-d^4/8 + d^3/6 + d^2/4 + d/6 + 1/24$
$0 \dots T$	$d^4/8 - d^3/3 + 2d/3 - 1/2$
$T \dots 2T$	$-d^4/24 + d^3/6 - d^2/4 + d/6 - 1/24$

smooth joints and converge to a Gaussian curve as the interpolation order increases. While the Lagrange interpolation polynomials or their derivatives have discontinuities between segments, the B-spline interpolation polynomials are continuous up to $(N - 1)$ th order derivatives, because they are built on successive convolutions of the rectangular pulse. Applying the convolution theorem and knowing that the Fourier transform of a rectangular pulse is a sinc function results in the Fourier transform of the N th-order B-spline interpolation polynomial

$$B_N(\omega) = \text{sinc}^{N+1}\left(\frac{\omega}{2\pi}\right). \quad (20)$$

Therefore, the spectra of B-spline interpolation polynomials decay faster than those of the same-order Lagrange interpolation polynomial, implying that the bandlimited step function using the B-spline interpolation can suppress aliasing more effectively.

Figure 8 shows two sawtooth waveforms and their spectra using the B-spline PolyBLEP method. Compared to the spectra in Fig. 5, aliasing is reduced more, given by the

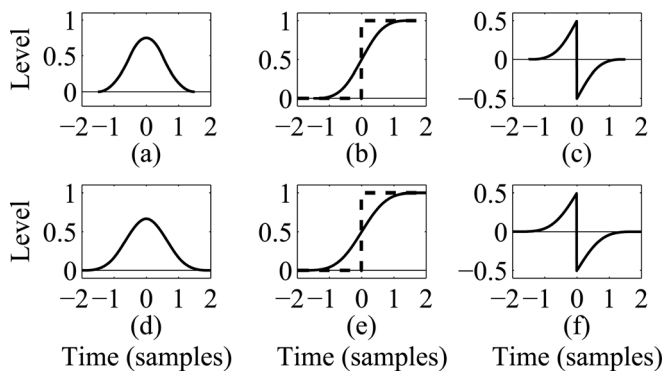


FIG. 7. Continuous-time impulse responses of the (a) second-order and (d) third-order B-spline interpolation, the corresponding integrated impulse responses (solid line) together with the unit step function (dashed line) in (b) and (e), and the corresponding BLEP residuals in (c) and (f).

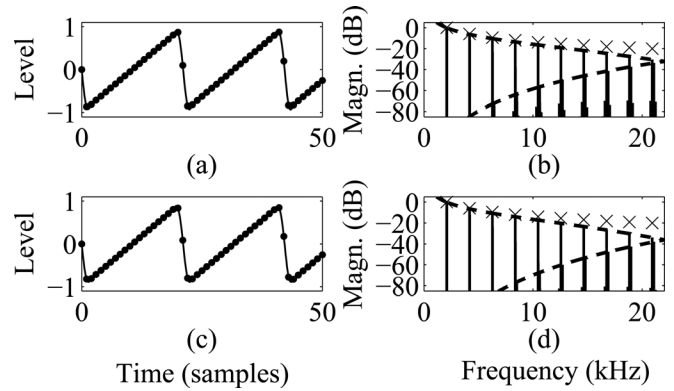


FIG. 8. Sawtooth waveforms produced by the (a) third-order and (c) fourth-order B-spline PolyBLEP methods and their respective magnitude spectra (b) and (d).

power of the sinc function. However, the desired harmonic components at high frequencies are reduced more in Fig. 8 than in Fig. 5. Again, an equalizing filter can be used to boost the level of harmonics at high frequencies. The two coefficients of the second-order FIR filter of Eq. (16) were optimized for the B-spline PolyBLEPs of order 3 and 4, see Table IV. Using the equalizing filter, the harmonic levels do not deviate more than 1 dB from the ideal.

Again, it can be noted that the odd-order B-spline PolyBLEPs are computationally, at least, as complex as the computation of the higher even-order B-spline PolyBLEP correction function. Thus, it is highly recommended to use even-order B-spline PolyBLEPs.

IV. EVALUATION OF THE PROPOSED ALGORITHMS

As shown in Figs. 5 and 8, the proposed PolyBLEP algorithms are not perfectly bandlimited and they still contain some aliasing. However, the aliasing may not be perceived by the human hearing system in certain conditions due to a psychoacoustic phenomenon called frequency masking.⁵⁰ An aliased component with sufficiently low amplitude can be masked in the sensory system by a near-enough harmonic peak so that the aliased component is not perceived. In addition, if an aliased component is not masked by the harmonic components but its level is low, it may become masked by the hearing threshold. This phenomenon is common especially at frequencies above 15 kHz, where the hearing threshold increases dramatically.⁵⁰

A. The highest aliasing-free fundamental frequency

In the evaluation of the sound quality of the proposed algorithms, the audibility of aliasing could be investigated by performing a listening test for a group of subjects. However, such subjective tests are dependent on the listening conditions. Therefore, an objective analysis for the proposed algorithms is conducted in this paper. In the objective analysis, the masking phenomena caused by frequency masking and the hearing threshold are incorporated by investigating whether there is any aliasing above the maximum of the masking thresholds of the desired harmonic components and the hearing threshold. Here, computational models of the hearing threshold and the

frequency masking approximated from experimental data are exploited.⁵⁰ The same perceptual evaluation method has previously been used by Nam *et al.*³⁶ and Välimäki *et al.*²⁹

The hearing threshold is given as the absolute sound-pressure level (SPL) by

$$T(f) = 3.64 \left(\frac{f}{1000} \right)^{-0.8} - 6.5 \exp \left(-0.6 \left(\frac{f}{1000} - 3.3 \right)^2 \right) + 10^{-3} \left(\frac{f}{1000} \right)^4, \quad (21)$$

where f is the frequency in Hz.⁵¹ Frequency masking is modeled as a spread function for a masker, as given by an asymmetric function⁵²

$$S(L_M, \Delta z_b) = L_M + (-27 + 0.37 \max\{L_M - 40, 0\}) \times \theta(\Delta z_b) |\Delta z_b|, \quad (22)$$

where L_M is the SPL of a masker in dB, Δz_b is the difference between the frequencies of a masker and a maskee in Bark units, and $\theta(\Delta z_b)$ is the step function equal to zero when $\Delta z_b < 0$ and equal to one when $\Delta z_b \geq 0$. The spreading functions given by Eq. (22) set their peaks equal to the levels of the maskers. To match the experimental data, they are shifted down depending on the type of the masker. For a tonal masker the downshift is greater than for a noise-like masker. As a bandlimited oscillator contains nearly tonal maskers, the downshift level is set to 10 dB.⁵³ Furthermore, to have consistent analysis results, the spectral power of the oscillators is scaled to a reference SPL. For the reference level the power of a sinusoid alternating between -1 and 1 was chosen, matching to a SPL of 96 dB, which is a common choice in audio coding.

Figure 9 shows the spectra of sawtooth waveforms corrected with the second-, third-, and fourth-order Lagrange PolyBLEP approaches with a fundamental frequency of 6645 Hz using the described objective analysis approach. Equalizing filters are not used here or in any other evaluation in this paper. The maximum of the hearing threshold and the masking threshold of the desired components is plotted with a dashed line in Fig. 9. As can be seen, all Lagrange approaches have some aliased components above the audibility threshold, as indicated with circles. As the order increases, the level of the aliased components is decreased. The analysis for the third- and fourth-order B-spline PolyBLEP approaches is shown in Fig. 10. Now, the third-order B-spline PolyBLEP contains some audible aliasing but the fourth-order case is aliasing-free, see Fig. 10(b).

By comparing Figs. 9 and 10 it appears that the B-spline PolyBLEP approach is slightly better than the Lagrange approach of the same order. In order to qualify this perception, the highest fundamental frequency up to which the aliasing is below the masking threshold was identified for a sawtooth waveform generated by the proposed PolyBLEP algorithms. The highest aliasing-free fundamental frequencies are listed in Table VIII for the PolyBLEP approaches and for three different lengths of a BLEP approach implemented as a look-up table made of a windowed and over-

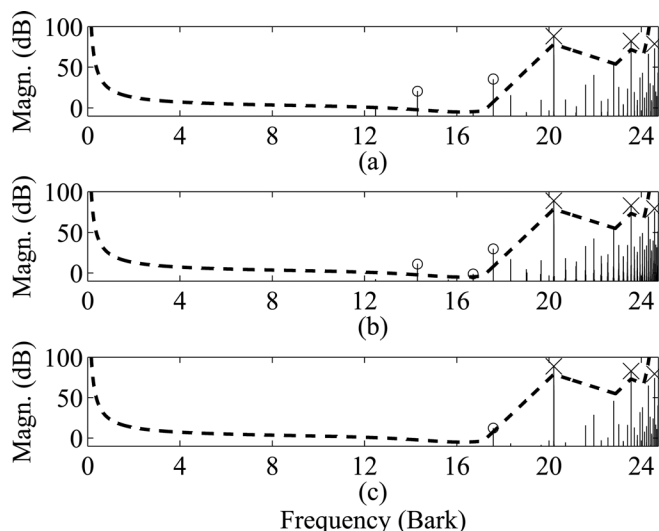


FIG. 9. Spectrum of a sawtooth wave with fundamental frequency of 6645 Hz using the sample rate of 44.1 kHz corrected with the (a) second-order, (b) third-order, and (c) fourth-order Lagrange PolyBLEP approach. The desired magnitudes of the non-aliased components are marked with crosses. The dashed line represents the maximum of the hearing threshold and the masking threshold of the non-aliased components, assuming that the sawtooth wave is played back at 96 dB SPL. The aliased components above the perceptual threshold are indicated with circles.

sampled ideal BLEP residual. In the look-up table BLEP approach (LUT-BLEP), the cut-off frequency scaling factor of $\alpha = 1$, an oversampling factor of 64, and a Blackman window were used.

As can be seen in Table VIII, the second-order PolyBLEP is free from aliasing up to about 2 kHz above which there is only one octave in a piano keyboard range (from 27.5 Hz to 4.2 kHz). Therefore, the second-order PolyBLEP can be considered aliasing-free in the frequency range of interest in most musical applications. It can also be verified that the highest aliasing-free fundamental frequency increases as the order of the correction polynomial increases and that the B-spline PolyBLEP approach is better than the Lagrange approach of the same order. The third-order B-spline PolyBLEP and both fourth-order PolyBLEPs are free of aliasing in the entire piano range. It should also be noted that the fourth-order B-spline PolyBLEP is aliasing-free up

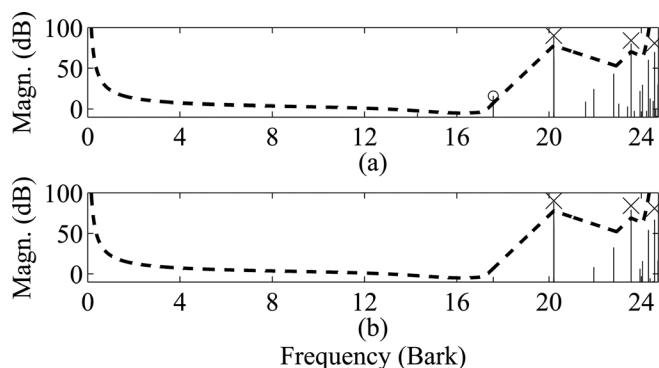


FIG. 10. Spectrum of a sawtooth wave with fundamental frequency of 6645 Hz corrected with the (a) third-order and (b) fourth-order B-spline PolyBLEP methods.

TABLE VIII. Highest fundamental frequency that is perceptually aliasing-free for a sawtooth signal corrected with a polynomial (Lagrange and B-spline) or a look-up table BLEP (LUT-BLEP) method. In the LUT-BLEP residuals, the cut-off frequency scaling factor of $\alpha = 1$, an oversampling factor of 64, and a Blackman function were used, and K indicates the number of samples to be corrected.

Correction function	Fundamental frequency
LUT-BLEP, $K = 4$	358 Hz
LUT-BLEP, $K = 32$	2036 Hz
PolyBLEP, $N_1 = 2$	2135 Hz
Lagrange PolyBLEP, $N_1 = 3$	3236 Hz
B-spline PolyBLEP, $N_1 = 3$	4591 Hz
LUT-BLEP, $K = 64$	4595 Hz
Lagrange PolyBLEP, $N_1 = 4$	5134 Hz
B-spline PolyBLEP, $N_1 = 4$	7845 Hz

to almost 8 kHz. At that fundamental frequency the signal contains only two harmonic components in the human hearing range.

Furthermore, as the fourth-order PolyBLEPs modify only four samples around the waveform transition, the highest aliasing-free fundamental frequency for a LUT-BLEP approach that also modifies only four samples was sought for comparison. One can see in Table VIII that the result for the corresponding LUT-BLEP is only a fraction of the highest aliasing-free fundamental frequency of the fourth-order PolyBLEP approaches. Increasing the number of samples to be modified in the LUT-BLEP approach to 32 makes its highest aliasing-free fundamental frequency to be comparable to the second-order polynomial approach. Yet, if the number of samples to be modified in the LUT-BLEP approach is increased to 64, the result becomes somewhat comparable to the third-order PolyBLEP approaches. Clearly, the windowed, over-sampled BLEP residual cannot compete with the polynomial approximations proposed in this work.

Comparing the results of Table VIII to the highest aliasing-free fundamental frequency of a sawtooth waveform obtainable by a BLIT algorithm utilizing the third-order B-spline interpolator as the bandlimited impulse (4593 Hz),³⁶ it is noted that the integration before the synthesis phase (as done in the BLEP approach) produces better alias reduction performance with polynomial approximations having the same order. This has been noted to be the case for the look-up table approaches.³⁹

B. Computational analysis on the level of aliasing

The level of aliasing as a function of the fundamental frequency can be investigated by computing a perceptual measure that takes into account the audible aliasing at all frequency bands. For such analysis there exist two standard measures, perceptual evaluation of audio quality (PEAQ)⁵⁴ and noise-to-mask ratio (NMR),^{55,56} which both compare the alias-corrupted signal to a clean, ideally bandlimited signal. Both of these measures were computed for the proposed approaches.

However, the PEAQ analysis produced results that were inconsistent with the observations made above about the audibility of aliasing. For example, the sawtooth wave with

fundamental frequency 41.2 Hz (note E1) produced by the four-point LUT-BLEP approach is supposed to be aliasing-free according to our analysis, but this signal received a PEAQ score about two grades lower than the other sawtooth waves below 77.8 Hz. Similarly ambiguous PEAQ analysis results were obtained for other compared algorithms at different frequency ranges. These observations raise the question of whether PEAQ is meaningful for analyzing the audible disturbance caused by aliasing, and therefore it was dropped from further investigations.

The NMR results were consistent and matched quite well with the analysis presented in Figs. 9 and 10. The NMR is computed by comparing the alias-corrupted signal to a band-limited reference signal composed using the additive synthesis approach¹⁰ from estimated amplitudes and phases of the harmonics of the corrupted signal in order to avoid errors. More specifically, the algorithm uses the error signal, i.e., the difference between the corrupted and aliasing-free signals. For both the error and the bandlimited signals a 1024-point magnitude spectrum is computed with FFT using the Hann window. In order to approximate the critical bands of hearing, the spectra are divided into segments for each of which an average energy is computed and converted to the decibel scale. A fraction of the energy from each critical band is copied to the neighboring bands using an interband spreading function to simulate the frequency masking phenomenon. The hearing threshold is taken into account as an additive term. Finally, the resulting energy for each band is computed, energies of all bands are summed, and a single NMR figure is described as the ratio of the error to the mask threshold computed using the operations given above. In the evaluation given in this paper, the sample rate of 44.1 kHz was used. The choice of the sample rate affects the choice of critical bands and spreading functions. In NMR figures, smaller values are considered better, and in NMR evaluations, often performed in audio coding applications, the NMR values below -10 dB are considered to be free from audible artifacts.⁵⁶

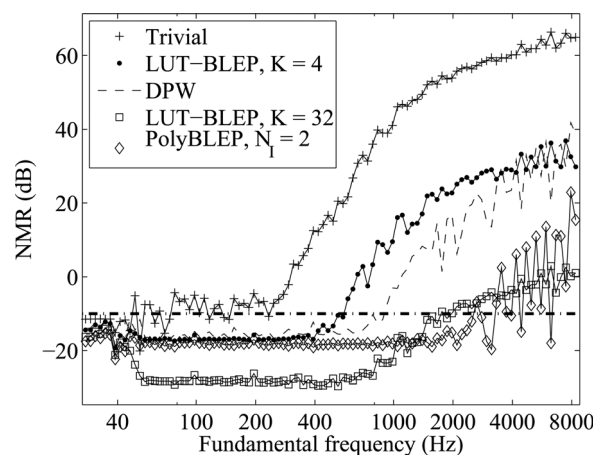


FIG. 11. Noise-to-mask ratio (NMR) figures for sawtooth waveforms obtained by trivial sampling (plus signs), four- (dots) and 32-point (squares) look-up table BLEP method (LUT-BLEP), and the second-order Lagrange PolyBLEP method (diamonds) as a function of the fundamental frequency. The NMR of the second-order DPW algorithm is plotted with dashed line for comparison.

Figure 11 presents the NMR figures as a function of the fundamental frequency for a trivially sampled sawtooth (plus signs), for LUT-BLEP approaches modifying four (dots) and 32 (squares) samples around the transition, for the second-order PolyBLEP approach (diamonds), and for the second-order differentiated polynomial (parabolic) waveform (DPW)^{25,29} approach (dashed line). In LUT-BLEP, the cut-off frequency scaling factor of $\alpha = 1$, an oversampling factor of 64, and a Blackman window were used. Note again that the second-order PolyBLEP method corresponds to integrated linear interpolation, which is the same as first-order Lagrange and first-order B-spline interpolation. For the analysis, fundamental frequencies from the lowest piano key up to an octave above the highest piano key were considered.

As can be seen in Fig. 11, the second-order PolyBLEP approach is below the -10 dB threshold up to over 2 kHz, that is clearly higher than the threshold crossing of, for instance, the second-order DPW algorithm approximately at 900 Hz. At 2 kHz, the second-order PolyBLEP produces an improvement of over 30 dB when compared to the second-order DPW algorithm and about 70 dB when compared to the trivial sampling. At 8 kHz, the improvement is smaller, still being about 20 dB when compared to the second-order DPW and 40 dB when compared to the trivial sampling. Figure 11 also shows that a LUT-BLEP approach modifying four samples provides NMR figures comparable to the second-order DPW algorithm. The number of samples to be modified in the LUT-BLEP approach must be increased to 32 in order to have NMR figures that are comparable to the second-order PolyBLEP approach.

The NMR figures for third-order Lagrange (triangles), fourth-order Lagrange (crosses), third-order B-spline (circles), and fourth-order B-spline PolyBLEP approaches (stars) are shown in Fig. 12. As can be seen, the NMR figures of all these PolyBLEP approaches are below the -10 dB threshold up to 4 kHz. Above 4 kHz, the NMR figures decrease as the order of the PolyBLEP approach increases. Furthermore, the B-spline PolyBLEP approaches [Fig. 12(b)] have smaller NMR figures than the Lagrange approach [Fig. 12(a)] of the

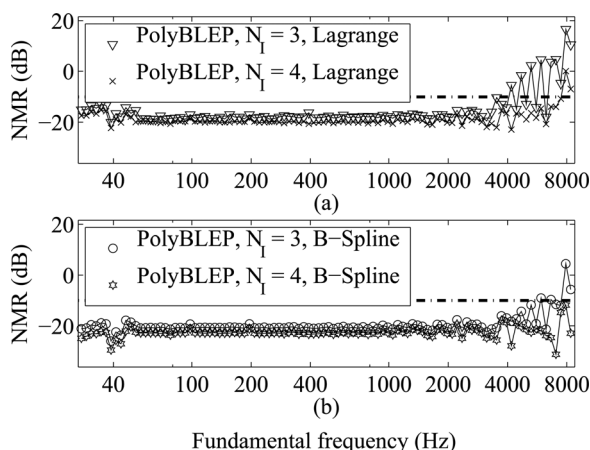


FIG. 12. NMR figures for sawtooth waveforms obtained by (a) the third-order Lagrange (triangles), the fourth-order Lagrange (crosses), (b) the third-order B-spline (circles), and the fourth-order B-spline PolyBLEP methods (stars).

same orders. The third-order Lagrange PolyBLEP crosses the -10 dB threshold around 4 kHz whereas the third-order B-spline PolyBLEP stays below the threshold up to 5 kHz. The fourth-order Lagrange PolyBLEP goes above the threshold at around 7.5 kHz while the fourth-order B-spline PolyBLEP remains below at all evaluated fundamental frequencies.

From Figs. 11 and 12 it can be concluded that a low-order polynomial correction function can be efficiently used in the reduction of aliasing in digital classical waveform synthesis. The second-order PolyBLEP is sufficient, apart from the highest octave of the piano range, and any higher-order PolyBLEP can be considered to be aliasing-free in the entire piano range. If the frequency range of interest is extended one octave above the piano range, the fourth-order B-spline PolyBLEP provides an aliasing-free oscillator.

C. Estimation of the computational load

The number of operations required in addition to the trivial waveform generation in one period of oscillation for the second- and fourth-order PolyBLEP algorithms are listed in Table IX. As can be seen, the number of additional operations is about the same for both fourth-order approaches. The third-order polynomial correction functions require different amounts of additional operations depending on the range of the fractional delay (cf. Tables II and VI) and were therefore ignored in the listing. In addition to the operations listed in Table IX, the PolyBLEP approach also requires a multiplication to determine the fractional delay of the transition, see Eq. (13). However, if the fundamental frequency changes from the previous discontinuity, a division is required. It should be noted that Table IX includes the additions needed in applying the correction function to the trivial waveform.

In the LUT-BLEP approach, where the correction function is read from a table, the computation of a single correction sample requires two reads from the residual table, two multiplications and two additions if linear interpolation is utilized to improve accuracy. Furthermore, when an oversampled table is used, the computation of the correct locations of the table reads requires one additional multiplication. The overall numbers of additional operations are then $2K$ reads, $2K + 1$ multiplications, and $2K$ additions for the computation of the correction function of length K . Applying the correction function to the trivial waveform increases the number of additions by K . As with the PolyBLEP approach, the computation of the fractional delay requires a multiplication or a division, depending on whether the fundamental frequency has changed or not.

TABLE IX. Additional operations required in even-order PolyBLEP approaches with respect to the trivial signal generation in one period of oscillation.

PolyBLEP function	Multiplications	Additions
PolyBLEP, $N_1 = 2$	4	4
Lagrange PolyBLEP, $N_1 = 4$	14	15
B-spline PolyBLEP, $N_1 = 4$	13	15

When comparing the alias reduction performance of the PolyBLEP and the LUT-BLEP approaches, the number of required operations is greatly less in the PolyBLEP approach. For instance, the alias reduction performance obtained by the LUT-BLEP approach modifying 32 samples around the transitions can be achieved with the second-order PolyBLEP that requires 8 operations, whereas the LUT-BLEP requires almost 450 operations in total. Furthermore, whereas the number of required unit delays in the correction circuit of the PolyBLEP approach is equal to the order of the underlying interpolation polynomial, the LUT-BLEP approach requires $K - 1$ unit delays. When the overlapping of correction functions is undesirable, the highest obtainable fundamental frequency is clearly higher for the polynomial correction functions than for the LUT-BLEP correction functions having the same alias reduction performance. Therefore, the proposed methods, and especially the fourth-order B-spline PolyBLEP, are well suited for the synthesis of bandlimited digital classical waveforms when both the alias reduction performance and the number of additional operations are taken into account.

V. CONCLUSION

In this paper, an approach that suppresses the perceived aliasing in the digitally synthesized periodic geometric waveforms by applying a correction function to the non-bandlimited waveform as a post-processing step was investigated. The ideal correction function was derived in closed form and polynomial approximations of the ideal correction function were discussed. By using a polynomial correction function, look-up tables that are typically used to store the correction function are not needed. Furthermore, the temporal discretization associated with the tabulated correction functions is avoided and oversampling that improves the accuracy of the correction function positioning does not have to be considered. When using a polynomial correction function, the alias reduction performance can be improved by increasing the polynomial order. The polynomial correction functions are also computationally efficient to evaluate, because the polynomials are sparse and some of their coefficients have common terms.

It was shown that with the proposed polynomial correction functions, integrated Lagrange and B-spline interpolators, the aliasing at low and middle frequencies, where human hearing is most sensitive, is suppressed the most. Using a computational model of the audibility of aliasing it was shown that a sawtooth waveform corrected with a second-order correction function is aliasing-free when the fundamental frequency is less than 2.1 kHz when the sample rate of 44.1 kHz is used. With a fourth-order correction function the sawtooth is free from aliasing in the whole piano range (from 27.5 Hz to 4.2 kHz). In order to reach comparable results with the traditional tabulated correction function approach, the length of the correction table needs to modify over ten times more samples around each discontinuity than the polynomial method.

In addition to the highest aliasing-free fundamental frequency, the overall aliasing level at all frequency bands of

the proposed polynomial correction function approaches were evaluated using a standard computational perceptual sound quality measure called the noise-to-mask ratio. The noise-to-mask ratio measures showed similar results as the analysis of the highest aliasing-free fundamental frequency, and it was proven that the integrated B-spline interpolators provide a better alias reduction than the integrated Lagrange interpolators of the same order. According to the noise-to-mask ratio measures, the third-order B-spline and the fourth-order Lagrange-based polynomial correction functions are free from audible aliasing in the whole piano range and the fourth-order B-spline-based polynomial correction is aliasing-free up to one octave above the piano range.

ACKNOWLEDGMENTS

The authors would like to thank Professor Marina Bosi, Andreas Franck, and Dr. Tim Stilson for helpful discussions, and Luis Costa and Julian Parker for proofreading this paper. This work has been partly financed by the Academy of Finland (Project Nos. 122815 and 126310).

- ¹H. F. Olson and H. Belar, "Electronic music synthesis," *J. Acoust. Soc. Am.* **27**(3), 595–612 (1955).
- ²R. A. Moog, "Voltage-controlled electronic music modules," *J. Audio Eng. Soc.* **13**(3), 200–206 (1965).
- ³H. G. Alles, "Music synthesis using real time digital techniques," *Proc. IEEE* **68**(4), 436–449 (1980).
- ⁴F. R. Moore, *Elements of Computer Music* (Prentice-Hall, Englewood Cliffs, NJ, 1990), pp. 44–48.
- ⁵P. Burk, "Bandlimited oscillators using wave table synthesis," in *Audio Anecdotes II—Tools, Tips, and Techniques for Digital Audio*, edited by K. Greenebaum and R. Barzel (A. K. Peters, Wellesley, MA, 2004), pp. 37–53.
- ⁶M. Puckette, *The Theory and Technique of Electronic Music* (World Scientific, Hackensack, NJ, 2007), pp. 301–322.
- ⁷H. Chamberlin, *Musical Applications of Microprocessors*, 2nd ed. (Hayden Book Company, Hasbrouck Heights, NJ, 1985), pp. 418–480.
- ⁸G. Winham and K. Steiglitz, "Input generators for digital sound synthesis," *J. Acoust. Soc. Am.* **47**, 665–666 (1970).
- ⁹J. A. Moorer, "The synthesis of complex audio spectra by means of discrete summation formulas," *J. Audio Eng. Soc.* **24**(9), 717–727 (1976).
- ¹⁰A. Chaudhary, "Bandlimited simulation of analog synthesizer modules by additive synthesis," in *Proceedings of the Audio Engineering Society's 105th Convention*, San Francisco, CA, 1998, Paper No. 4779.
- ¹¹G. Deslauriers and C. Leider, "A bandlimited oscillator by frequency-domain synthesis for virtual analog applications," in *Proceedings of the Audio Engineering Society's 127th Convention*, New York, NY, 2009, Paper No. 7923.
- ¹²D. C. Massie, "Wavetable sampling synthesis," in *Applications of Digital Signal Processing to Audio and Acoustics*, edited by M. Kahrs and K. Brandenburg (Kluwer Academic, Norfolk, MA, 1998), pp. 311–341.
- ¹³J. Pekonen, "Computationally Efficient Music Synthesis—Methods and Sound Design," M.Sc.thesis, Helsinki University of Technology, Espoo, Finland, 2007. Available online at http://www.acoustics.hut.fi/publications/files/theses/pekonen_mst/ (Last viewed December 17, 2010).
- ¹⁴J. Timoney, V. Lazzarini, B. Carty, and J. Pekonen, "Phase and amplitude distortion methods for digital synthesis of classic analogue waveforms," in *Proceedings of the Audio Engineering Society's 126th Convention*, Munich, Germany, 2009, Paper No. 7792.
- ¹⁵V. Lazzarini and J. Timoney, "New perspectives on distortion synthesis for virtual analog oscillators," *Comput. Music J.* **34**(1), 28–40 (2010).
- ¹⁶M. Le Brun, "Digital waveshaping synthesis," *J. Audio Eng. Soc.* **27**(4), 250–266 (1979).
- ¹⁷D. Arfib, "Digital synthesis of complex spectra by means of multiplication of nonlinear distorted sine waves," *J. Audio Eng. Soc.* **27**(10), 757–768 (1979).
- ¹⁸M. Ishibashi, "Electronic musical instrument," U.S. Patent 4,658,691 (1987).

- ¹⁹V. Lazzarini, J. Timoney, J. Pekonen, and V. Välimäki, "Adaptive phase distortion synthesis," in *Proceedings of the 12th International Conference on Digital Audio Effects (DAFx-09)*, Como, Italy, 2009, pp. 28–35.
- ²⁰J. Timoney, V. Lazzarini, J. Pekonen, and V. Välimäki, "Spectrally rich phase distortion sound synthesis using an allpass filter," in *Proceedings of the IEEE International Conference on Acoustics, Speech, and Signal Processing*, Taipei, Taiwan, 2009, pp. 293–296.
- ²¹J. Kleimola, J. Pekonen, H. Penttinen, V. Välimäki, and J. S. Abel, "Sound synthesis using an allpass filter chain with audio-rate coefficient modulation," in *Proceedings of the 12th International Conference on Digital Audio Effects (DAFx-09)*, Como, Italy, 2009, pp. 305–312.
- ²²V. Lazzarini, J. Timoney, J. Kleimola, and V. Välimäki, "Five variations on a feedback theme," in *Proceedings of the 12th International Conference on Digital Audio Effects (DAFx-09)*, Como, Italy, 2009, pp. 139–145.
- ²³J. Kleimola, "Audio synthesis by bitwise logical modulation," in *Proceedings of the 11th International Conference on Digital Effects (DAFx-08)*, Espoo, Finland, 2008, pp. 67–70.
- ²⁴J. Lane, D. Hoory, E. Martinez, and P. Wang, "Modeling analog synthesis with DSPs," *Comput. Music J.* **21**(4), 23–41 (1997).
- ²⁵V. Välimäki, "Discrete-time synthesis of the sawtooth waveform with reduced aliasing," *IEEE Signal Process. Lett.* **12**(3), 214–217 (2005).
- ²⁶A. Huovilainen and V. Välimäki, "New approaches to digital subtractive synthesis," in *Proceedings of the International Computer Music Conference*, Barcelona, Spain, 2005, pp. 399–402.
- ²⁷V. Välimäki and A. Huovilainen, "Oscillator and filter algorithms for virtual analog synthesis," *Comput. Music J.* **30**(2), pp. 19–31 (2006).
- ²⁸D. Lowenfels, "Virtual analog synthesis with a time-varying comb filter," in *Proceedings of the Audio Engineering Society's 115th Convention*, New York, NY, 2003, Paper No. 5960.
- ²⁹V. Välimäki, J. Nam, J. O. Smith, and J. S. Abel, "Alias-suppressed oscillators based on differentiated polynomial waveforms," *IEEE Trans. Audio Speech Lang. Process.* **18**(4), 786–798 (2010).
- ³⁰J. Pekonen and V. Välimäki, "Filter-based alias reduction in classical waveform synthesis," in *Proceedings of the IEEE International Conference on Acoustics, Speech and Signal Processing*, Las Vegas, NV, 2008, pp. 133–136.
- ³¹T. Stilson and J. Smith, "Alias-free digital synthesis of classic analog waveforms," in *Proceedings of the International Computer Music Conference*, Hong Kong, China, 1996, pp. 332–335.
- ³²T. Stilson, "Efficiently-variable non-oversampling algorithms in virtual-analog music synthesis—A root-locus perspective," Ph.D. dissertation, Dept. of Electrical Eng., Stanford Univ., Stanford, CA, 2006. Available online at <http://ccrma.stanford.edu/~stilti/papers/> (Last viewed December 17, 2010).
- ³³J. Timoney, V. Lazzarini, and T. Lysaght, "A modified FM synthesis approach to bandlimited signal generation," in *Proceedings of the 11th International Conference on Digital Audio Effects (DAFx-08)*, Espoo, Finland, 2008, pp. 27–33.
- ³⁴J. Nam, V. Välimäki, J. S. Abel, and J. O. Smith, "Alias-free oscillators using feedback delay loops," in *Proceedings of the 12th International Conference on Digital Audio Effects (DAFx-09)*, Como, Italy, 2009, pp. 347–352.
- ³⁵J. Pekonen, V. Välimäki, J. Nam, J. O. Smith, and J. S. Abel, "Variable fractional delay filters in bandlimited oscillator algorithms for music synthesis," in *Proceedings of the 2010 International Conference on Green Circuits and Systems (ICGCS2010)*, Shanghai, China, 2010, pp. 148–153.
- ³⁶J. Nam, V. Välimäki, J. S. Abel, and J. O. Smith, "Efficient antialiasing oscillator algorithms using low-order fractional delay filters," *IEEE Trans. Audio Speech Lang. Process.* **18**(4), 773–785 (2010).
- ³⁷J. Pekonen, J. Nam, J. O. Smith, J. S. Abel, and V. Välimäki, "On minimizing the look-up table size in quasi bandlimited classical waveform synthesis," in *Proceedings of the 13th International Conference on Digital Audio Effects (DAFx-10)*, Graz, Austria, 2010, pp. 57–64.
- ³⁸E. Brandt, "Hard sync without aliasing," in *Proceedings of the International Computer Music Conference*, Havana, Cuba, 2001, pp. 365–368.
- ³⁹V. Välimäki and A. Huovilainen, "Antialiasing oscillators in subtractive synthesis," *IEEE Signal Process. Mag.* **24**(2), 116–125 (2007).
- ⁴⁰A. B. Leary and C. T. Bright, "Bandlimited digital synthesis of analog waveforms," U.S. Patent 7,589,272 (2009).
- ⁴¹M. Abramowitz and I. A. Stegun, editors, *Handbook of Mathematical Functions with Formulas, Graphs, and Mathematical Tables* (U.S. Department of Commerce, Washington DC, 1964), available online at http://www.knovel.com/web/portal/basic_search/display7_EXT_KNOVEL_DISPLAY_bookid=528, pp. 231–232 (Last viewed December 17, 2010).
- ⁴²O. D. Grace, "Polynomial interpolation of bandlimited signals," *J. Acoust. Soc. Am.* **54**(3), 807–808 (1973).
- ⁴³R. W. Schafer and L. R. Rabiner, "A digital signal processing approach to interpolation," *Proc. IEEE* **61**(6), 692–702 (1973).
- ⁴⁴H. W. Strube, "Sampled-data representation of a nonuniform lossless tube of continuously variable length," *J. Acoust. Soc. Am.* **57**(1), 256–257 (1975).
- ⁴⁵T. I. Laakso, V. Välimäki, M. Karjalainen, and U. K. Laine, "Splitting the unit delay—Tools for fractional delay filter design," *IEEE Signal Process. Mag.* **13**(1), 30–60 (1996).
- ⁴⁶A. Franck, "Efficient algorithms and structures for fractional delay filtering based on Lagrange interpolation," *J. Audio Eng. Soc.* **56**(12), 1036–1056 (2008).
- ⁴⁷E. Hermanowicz, "Explicit formulas for weighting coefficients of maximally flat tunable FIR delayers," *Electron. Lett.* **28**(20), 1936–1937 (1992).
- ⁴⁸A. Franck and K. Brandenburg, "A closed-form description for the continuous frequency response of Lagrange interpolators," *IEEE Signal Process. Lett.* **16**(7), 612–615 (2009).
- ⁴⁹M. Unser, "Splines: A perfect fit for signal and image processing," *IEEE Signal Process. Mag.* **16**(6), 22–38 (1999).
- ⁵⁰E. Zwicker and H. Fastl, *Psychoacoustics* (Springer-Verlag, Berlin, 1990), pp. 15–19, 56–102.
- ⁵¹E. Terhardt, "Calculating virtual pitch," *Hearing Res.* **1**(2), 155–182 (1979).
- ⁵²M. Bosi, "Audio coding: Basic principles and recent developments," in *Proceedings of the 6th International Conference on Humans and Computers*, Aizu, Japan, 2003, pp. 1–17.
- ⁵³M. Lagrange and S. Marchand, "Real-time additive synthesis of sound by taking advantage of psychoacoustics," in *Proceedings of the COST G-6 Conference on Digital Audio Effects (DAFx-01)*, Limerick, Ireland, 2001, pp. 5–9.
- ⁵⁴International Telecommunication Union, "Method for Objective Measurement of Perceptual Audio Quality," Recommendation ITU-R BS No. 1387, 1998.
- ⁵⁵K. Brandenburg, "Evaluation of quality for audio encoding at low bit rates," in *Proceedings of the Audio Engineering Society's 82nd Convention*, London, UK, 1987, Paper No. 2433.
- ⁵⁶K. Brandenburg and T. Sporer, "'NMR' and 'Masking Flag': Evaluation of quality using perceptual criteria," in *Proceedings of the Audio Engineering Society's 11th International Conference on Test and Measurement*, Portland, OR, 1992, pp. 169–179.